J Solid State Electrochem (2005) 9: 83–90
DOI 10.1007/s10008-004-0557-2

ORIGINAL PAPER

Joan Gregori · José J. García-Jareño
David Giménez-Romero · Francisco Vicente

Kinetic calculations of the Ni anodic dissolution from EIS

Received: 17 October 2003 / Accepted: 25 March 2004 / Published online: 9 July 2004

Abstract Anodic nickel dissolution in acid media has been analyzed by means of electrochemical quartz crystal microbalance and electrochemical impedance spectroscopy techniques. The experimental impedance spectra have been fitted to an equivalent circuit which is related to a mechanism of two consecutive electron transfers followed by a Ni^{2+} mass transfer step. That way, an estimation for values of rate constants and surface concentrations of the Ni(0), Ni(I) and Ni(II) species has been obtained.

Keywords Electrochemical impedance spectroscopy · Electrochemical quartz crystal microbalance · Consecutive electron transfers · Anodic dissolution of nickel

Introduction

Nickel is an essential metal from an industrial point of view. It is widely used in many alloys and occurs in several common objects and devices [1, 2]. But it is also the origin of many health problems related to allergic and oncology diseases. This is why nickel has been the subject of many researches related to dissolution and passivation mechanisms in acid medium by means of different electrochemical techniques [3, 4, 5, 6, 7, 8, 9, 10, 11]. However, several points remain unclear due to the strong tendency for self-passivation of nickel and, in that way, the process of active dissolution, passive layer formation and chemical dissolution depends on a great number of variables: history of the electrodes, media, roughness of the surface, hydrodynamic conditions, metal impurities on the surface, etc [4].

J. Gregori · J. J. García-Jareño · D. Giménez-Romero
F. Vicente (✉)
Department of Physical Chemistry,
University of Valencia, C/ Dr. Moliner 50,
46100 Burjassot, Spain
E-mail: proclq@uv.es

According to the EQCM (electrochemical quartz crystal microbalance) results obtained by Itagaky et al. at potentiostatic conditions [11], two consecutive electron transfers can be considered for the early stages of nickel electrodissolution, as is frequently postulated in the electrodissolution of other similar metals under certain experimental conditions [7, 8, 9, 11, 12, 13, 14]:

$$\mathrm{Ni(0)}(\theta_0) \xrightarrow{k_1} \mathrm{Ni(I)}(\theta_1) + \mathrm{e}^- \tag{1}$$

$$\mathrm{Ni(I)}(\theta_1) \xrightarrow{k_2} \mathrm{Ni(II)}(\theta_2) + \mathrm{e}^- \tag{2}$$

$$\mathrm{Ni(II)}(\theta_2) \xrightarrow{k_3} \mathrm{Ni}^{2+} \tag{3}$$

where θ_0, θ_1 and θ_2 are the surface concentrations of Ni(0), Ni(I) and Ni(II) species, respectively and Ni^{2+} is the nickel in the solution. The first and the second steps are two consecutive irreversible single-electron transfers and the third one is a physical process that consists of the solubilization of Ni (II) species and transport of Ni^{2+} throughout the aqueous media.

Electrochemical impedance spectroscopy (EIS) is a technique which allows kinetic information to be obtained about the processes which take place on an electrode surface at a steady state potential [15, 16, 17, 18, 19, 20, 21, 22, 23]. If it is considered that the kinetic constants for the electrochemical steps follow a Butler–Volmer relationship and the elementary steps obey first-order kinetics, then the rates for each elemental step can be expressed as:

$$r_1 = k_{01}\theta_0 \mathrm{e}^{b_1 E} \tag{4}$$

$$r_2 = k_{02}\theta_1 \mathrm{e}^{b_2 E} \tag{5}$$

$$r_3 = k_{03}\theta_2 \tag{6}$$

The mass balance and the charge balance at the electrode surface are:

$$\frac{i_F}{F} = r_1 + r_2 \tag{7}$$

$$\frac{d\theta_0}{dt} = r_3 - r_1 \tag{8}$$

$$\frac{d\theta_1}{dt} = r_1 - r_2 = k_1\theta_0 - k_2\theta_1 \tag{9}$$

$$\frac{d\theta_2}{dt} = r_2 - r_3 = k_2\theta_1 - k_3\theta_2 \tag{10}$$

where r_i and k_i are the rates and their respective rate constants of the postulated steps. E is the applied potential, i_F is the faradaic current intensity and F is the Faraday constant.

From Eqs. (7), (9) and (10) the theoretical faradaic impedance for the above reaction mechanism can be deduced in different manner [24, 25] (see Appendix 1 for more details) following Armstrong's formalism [26]:

$$FZ_F = \left[\frac{\partial r_1}{\partial\theta_0}\frac{\partial r_2}{\partial\theta_1} + \left(\frac{\partial r_1}{\partial\theta_0} + \frac{\partial r_2}{\partial\theta_1}\right)\frac{\partial r_3}{\partial\theta_2} + \left(\frac{\partial r_1}{\partial\theta_0} + \frac{\partial r_2}{\partial\theta_1} + \frac{\partial r_3}{\partial\theta_2}\right)j\omega - \omega^2\right] \times \left[2\frac{\partial r_2}{\partial E}\frac{\partial r_1}{\partial\theta_0}\frac{\partial r_3}{\partial\theta_2} + 2\frac{\partial r_1}{\partial E}\frac{\partial r_2}{\partial\theta_1}\frac{\partial r_3}{\partial\theta_2} + \left(\frac{\partial r_2}{\partial E}\frac{\partial r_1}{\partial\theta_0} + 2\frac{\partial r_1}{\partial E}\frac{\partial r_2}{\partial\theta_1} + \frac{\partial r_1}{\partial E}\frac{\partial r_3}{\partial\theta_2} + \frac{\partial r_2}{\partial E}\frac{\partial r_3}{\partial\theta_2}\right)j\omega - \left(\frac{\partial r_1}{\partial E} + \frac{\partial r_2}{\partial E}\right)\omega^2\right]^{-1} \tag{11}$$

where F is the Faraday constant and Z_F is the Faradaic impedance.

The aim of this work is to calculate the kinetic parameters of the electrochemical dissolution of nickel in an acid medium from the electrochemical impedance results. The objective is to try a methodology for obtaining an approximate way of characterizing this complex process.

Experimental

All the experiments have been carried out in a typical three-electrode cell. The potential was measured versus a SSE (saturated sulfate electrode $Hg/Hg_2SO_4/K_2SO_4$ sat.) reference electrode of 0.656 V versus NHE at 298 K. A platinum sheet of a relative large area ($A = 2$ cm^2) was used as an auxiliary electrode. Solutions were prepared from K_2SO_4 (Probus, a.g.), H_2SO_4 (Merk, a.g.), KCl (Fluka, a.g.), $NiSO_4{\cdot}6H_2O$ (Scharlau, a.g.) with distilled and double deionized water (MilliQ).

For impedance measurements the potential was controlled with a potentiostat–galvanostat 273A EG&G PAR and the impedance spectra were recorded with the help of a lock-in amplifier 5210 EG&G PAR. The working electrodes were made from a nickel sheet (99.9%, Johnson and Matthey). The geometrical area was 0.25 cm^2. A potential of −1.250 V versus SSE was applied for 15 min and a potential of stabilization E_0 was applied for 60 min before recording the impedance spectra. The impedance measurements were carried out in the frequency range [10^5, 5×10^{-2}] Hz and the amplitude of the harmonic potential perturbation was 10 mV r.m.s. All the measurements were carried out at constant and controlled temperature $T = 298.5 \pm 0.1$ K. All solutions were deareated by bubbling Ar (from "Air Liquide") for 5 min before starting the experiment. All the impedance measurements have been performed under an inert atmosphere and still conditions. The fitting of experimental impedance data to the proposed equivalent circuit was carried out by means of a non-linear least squares procedure based on the Marquardt algorithm for function optimization [27, 28].

For EQCM experiments the working electrodes were made from a quartz sheet (quartz was supplied by Matel–Fordahl) embedded between two pieces of gold connected to a resonance circuit. The resonance frequency of the quartz in air was 6 MHz. The electrochemical active area was 0.228 cm^2 and the resonant area of quartz was 0.196 cm^2. The potential sweep was carried out from 0.200 to −1.500 V (versus SSE) at 0.020 V/s. The upper anodic potential is limited in order to avoid the gold electrode oxidation and the lower cathodic potential is limited in order to avoid the presence of hydrogen bubbles on the Au electrode and to improve the nickel electrodeposition/hydrogen evolution ratio [29]. Before starting the potential sweep the potential was kept constant at 0.200 V for 2 min. The microbalance was a UPR15/RT0100 (UPR of the CNRS). The resonance frequency of quartz was measured with a Fluke PM6685. The current in the auxiliary electrode was measured with a Keithley PM2000 multimeter. The potential was applied with a potentiostat 263A EG&G PAR. The whole system was controlled with a GPIB board. The EQCM was calibrated by means of a galvanostatic Cu deposition [30]. The nickel deposit obtained in this work was very thin, about 0.3 μm, where no non-ideal contributions are expected and Sauerbreys' equation applies. The experimental Sauerbrey constant was 9.50×10^7 Hz g^{-1}. According to Sauerbreys' equation [31], the mass changes on the electrode surface are related to the resonance frequency changes as follows:

$$\Delta f = -\frac{2f_0^2}{A\sqrt{E_y\rho}}\Delta m_e \tag{12}$$

where ρ is the quartz density and E_y is the stretch constant of quartz. f_0 is the base resonance frequency.

EQCM in combination with voltammetry provides important information about the mechanism and stoichiometry in metal dissolution and deposition process by means of the mass/charge ratio defined by:

$$F\frac{\Delta m}{\Delta Q} = \sum_i \frac{M_{w_i}}{n_i}v_i \pm \Delta M_0 \tag{13}$$

where ΔM_0 is the contribution of mass changes due to uncharged species. M_{wi} is the molecular mass of a species i, which interchanges n_i electrons and v_i is the charge ratio due to process i. Equation (13) provides information about the global electrode process in a time or potential range.

In the same way as in EIS measurements, the electrolyte has been purged for 5 min with Ar so as to remove the dissolved oxygen and all the measurements have been made under an inert atmosphere.

Experimental results and discussion

EQCM measurements

The voltammogram and the mass change in the potential window 0.2 to −1.5 V for a nickel electrode in an acid medium, pH = 2.7, are plotted in Fig. 1. In the potential range −0.8 to −1.5 V in a cathodic scan and −1.5 to −1.4 V in an anodic one a considerable mass increase takes place most probably caused by nickel electrodeposition [29]. In the potential range −0.750 to −0.500 V a considerable mass decrease takes place. This potential range includes anodic peak I and so this mass decrease is due to nickel electrodissolution [29].

In the potential range of nickel electrodeposition for the successive cycles, the experimental value of the mass/charge ratio remains around -2 g mol^{-1}, which is much smaller than the theoretical value for electrodeposition of nickel according to the stoichiometry of the reaction:

$$Ni^{2+} + 2e^- \rightarrow Ni \qquad (14)$$

which is $F(\Delta m/\Delta Q)_{\text{theoretical}} = -29$ g mol^{-1}. The difference between the experimental and theoretical value in this potential range is due to the great contribution of the hydrogen evolution reaction [32] to the overall transferred charge ΔQ.

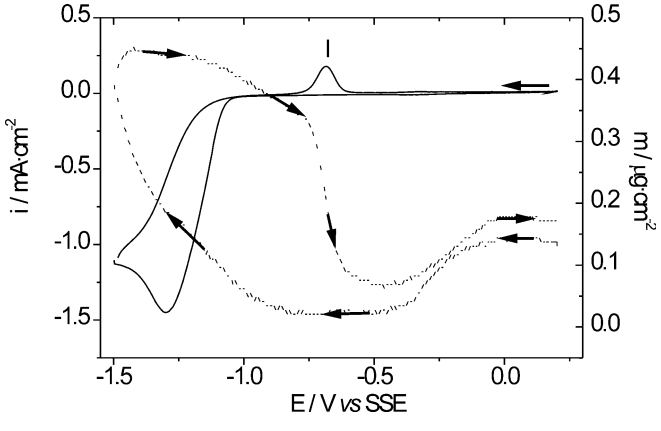

Fig. 1 Mass changes (*dashed line*) and voltammogram (*continuous line*) in the potential window [200, −1500] mV; scan rate = 20 mV/s; 10^{-3} M $NiSO_4$; 0.245 M K_2SO_4; 5×10^{-3} M H_2SO_4; pH = 2.7; T = 298 K

In the range of potentials where nickel electrodissolution takes place, the experimental value of the mass/charge ratio $F(\Delta m/\Delta Q)_{\text{theoretical}} = -38$ g mol^{-1} during the first voltammogram is higher than the theoretical value (−29 g mol^{-1}) which corresponds to a stoichiometric loss of one nickel atom for each of the two exchanged electrons. This calculated mass/charge ratio increases with the number of cycles. For instance, for the fifth cycle this ratio has a value of −45 g mol^{-1} and for the twentieth cycle it reaches a value of −52 g mol^{-1}. These results show the strong dependence of the dissolution mechanism on the previous activation electrode process. According to the work of Lachenwitzer et al. [33], a precursor for nickel electrodeposition is formed in cyclic voltammetry experiments. This precursor most probably is an Ni(I) species [34] that causes a modification of the nickel surface electrode.

Then, the most possible cause for the experimental fact that the mass/charge ratio increase with the number of potential cycles is directly related with the stabilization of an increasing amount of Ni(I) species on the electrode during the following cycles.

Calculation of kinetic parameters from EIS in the potential range of nickel dissolution

Figure 2 shows impedance spectra of nickel electrodissolution at different potentials. The theoretical faradaic impedance function, Eq. (11), is consistent with an equivalent circuit with two time constants, one for each reaction intermediate [35]. The experimental impedance spectra are fitted to the equivalent circuit of Fig. 2. R_1C_1 values will be related to relaxation of Ni(I) species and R_2C_2 values will be related to relaxation of Ni(II) species. R represents the charge transfer resistance. There is

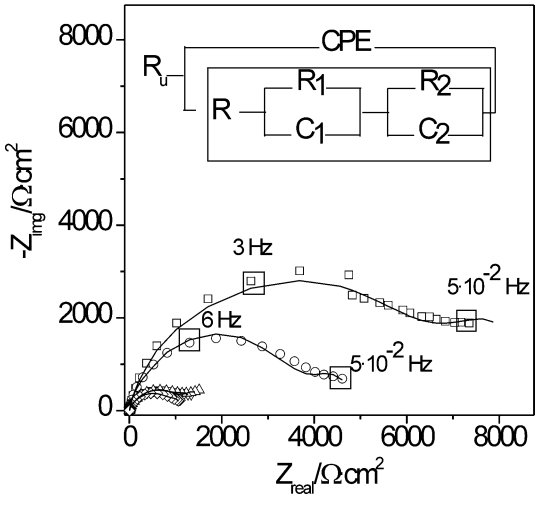

Fig. 2 Experimental impedance spectra at $E_0 = -650$ mV (*squares*), $E_0 = -600$ mV (*circles*), $E_0 = -585$ mV (*upward triangles*), $E_0 = -555$ mV (*downward triangles*) and $E_0 = -535$ mV (*diamonds*). 0.245 M K_2SO_4; 5×10^{-3} M H_2SO_4; pH = 2.7; T = 298 K. *Solid line* indicates the fitting to the equivalent circuit

a good agreement between experimental and fitted impedance spectra. In Table 1 the values of the equivalent circuit passive elements are presented.

In this sense, the low values obtained for the CPE exponent (approximately 0.8) can be explained by the roughness of the non-polished surface of nickel, and they can be also attributed to the formation of a new phase on the electrode surface during the electrodissolution process.

R values are very low (about 5 Ω cm^2) compared with R_1 and R_2 values and, consequently, R values calculated from the fitting have a great uncertainty. The uncompensated resistance, R_u, was calculated by extrapolating the impedance data to highest frequencies and it was found to be 3 ± 1 Ω cm^2 for all the samples tested.

From Eqs. (4), (5) and (6) each partial derivative is obtained:

$$\frac{\partial r_1}{\partial E} = b_1 k_{01} \theta_0 e^{b_1 E} \tag{15}$$

$$\frac{\partial r_1}{\partial \theta_0} = k_{01} e^{b_1 E} \tag{16}$$

$$\frac{\partial r_2}{\partial E} = b_2 k_{02} \theta_1 e^{b_2 E} \tag{17}$$

$$\frac{\partial r_2}{\partial \theta_1} = k_{02} e^{b_2 E} \tag{18}$$

$$\frac{\partial r_3}{\partial E} = 0 \tag{19}$$

$$\frac{\partial r_3}{\partial \theta_2} = k_{03} \tag{20}$$

The Faradaic impedance function for the equivalent circuit of Fig. 2 is:

$$Z_F = \frac{R + R_1 + R_2 + (R(R_1C_1 + R_2C_2) + R_1R_2(C_1 + C_2))j\omega - RR_1R_2C_1C_2\omega^2}{1 + (R_1C_1 + R_2C_2) - R_1R_2C_1C_2\omega^2} \tag{21}$$

If Eq. (21) and Eq. (11) are compared, an equation system for the partial derivatives (15)–(20) is obtained:

$$\frac{\frac{\partial r_1}{\partial \theta_0}\frac{\partial r_2}{\partial \theta_1} + \left(\frac{\partial r_1}{\partial \theta_0} + \frac{\partial r_2}{\partial \theta_1}\right)\frac{\partial r_3}{\partial \theta_2}}{2\frac{\partial r_2}{\partial E}\frac{\partial r_1}{\partial \theta_0}\frac{\partial r_3}{\partial \theta_2} + 2\frac{\partial r_1}{\partial E}\frac{\partial r_2}{\partial \theta_1}\frac{\partial r_3}{\partial \theta_2}} = F(R + R_1 + R_2) \tag{22}$$

$$\frac{\frac{\partial r_1}{\partial \theta_0} + \frac{\partial r_2}{\partial \theta_1} + \frac{\partial r_3}{\partial \theta 2}}{2\frac{\partial r_2}{\partial E}\frac{\partial r_1}{\partial \theta_0}\frac{\partial r_3}{\partial \theta_2} + 2\frac{\partial r_1}{\partial E}\frac{\partial r_2}{\partial \theta_1}\frac{\partial r_3}{\partial \theta_2}} = F\big(R(R_1C_1 + R_2C_2) + R_1R_2(C_1 + C_2)\big) \tag{23}$$

$$\frac{\frac{\partial r_1}{\partial \theta_0}\frac{\partial r_2}{\partial E} + 2\frac{\partial r_1}{\partial E}\frac{\partial r_2}{\partial \theta_1} + \frac{\partial r_1}{\partial E}\frac{\partial r_3}{\partial \theta_2} + \frac{\partial r_2}{\partial E}\frac{\partial r_3}{\partial \theta_2}}{2\frac{\partial r_2}{\partial E}\frac{\partial r_1}{\partial \theta_0}\frac{\partial r_3}{\partial \theta_2} + 2\frac{\partial r_1}{\partial E}\frac{\partial r_2}{\partial \theta_1}\frac{\partial r_3}{\partial \theta_2}} = R_1C_1 + R_2C_2 \tag{24}$$

$$\frac{\frac{\partial r_1}{\partial E} + \frac{\partial r_2}{\partial E}}{2\frac{\partial r_2}{\partial E}\frac{\partial r_1}{\partial \theta_0}\frac{\partial r_3}{\partial \theta_2} + 2\frac{\partial r_1}{\partial E}\frac{\partial r_2}{\partial \theta_1}\frac{\partial r_3}{\partial \theta_2}} = R_1R_2C_1C_2 \tag{25}$$

$$\frac{1}{2\frac{\partial r_2}{\partial E}\frac{\partial r_1}{\partial \theta_0}\frac{\partial r_3}{\partial \theta_2} + 2\frac{\partial r_1}{\partial E}\frac{\partial r_2}{\partial \theta_1}\frac{\partial r_3}{\partial \theta_2}} = FRR_1R_2C_1C_2 \tag{26}$$

which can be numerically solved for obtaining a first approach of the kinetics of the nickel dissolution process. However, this equation system can be simplified in order to improve its analytical solution if it is assumed that the system reaches the steady state.

The steady state condition applied to Eq. (9) allows one to obtain the relation $k_1\theta_0 = k_2\theta_1 = k_3\theta_2$. Thus, and taking into account the great uncertainty of R values, Eq. (26) can be suppressed from this equation system, since four non-dependent magnitudes are unknown if b_1 and b_2 are fixed.

Four approximate non-dependent equations are obtained if is considered that $C_1 \ll C_2$, $R \ll R_1$, R_2, and $k_1 \gg k_2$, k_3 too:

$$\frac{k_2 + k_3}{2k_1k_3b_2\theta_0} = F(R_1 + R_2) \tag{27}$$

$$\frac{1}{2k_1k_3b_2\theta_0} = F(R_1R_2C_2) \tag{28}$$

$$\frac{1}{2k_3} = R_1C_1 + R_2C_2 \tag{29}$$

$$\frac{b_1 + b_2}{2k_1k_3b_2} = R_1R_2C_1C_2 \tag{30}$$

Table 1 Determined values of the passive element of the equivalent circuit which result from the fitting procedure. The impedance of CPE is noted as $Z_{CPE} = 1/A(j\omega)^{\alpha}$. The calculated R values have a great uncertainty because they are very low with respect to the R_1 and R_2 values. The experimental conditions are the same as in Fig. 2

E (vs SSE) (mV)	A (μF cm^{-2} s$^{\alpha-1}$)	α	R_1(Ω cm^2)	C_1(μF cm^{-2})	R_2(Ω cm^2)	C_2(μF cm^{-2})
−650	20	0.82	7200	2	2750	840
−600	14	0.83	4000	3	1175	1280
−585	80	0.77	1250	3	600	2240
−555	150	0.79	1175	2	400	2960
−535	120	0.80	1000	3	250	3400

Table 2 Kinetic parameters, k_i, and surface concentration of Ni(0) species, θ_0, Ni(I) species, θ_1, and Ni(II) species, θ_2, on the electrode surface as a function of the applied potential. The experimental conditions are the same as in Fig. 2. In the presence of chloride (same experimental conditions as in Fig. 4)

E (mV)	$k_1(s^{-1})$	$k_2(s^{-1})$	$k_3(s^{-1})$	$\theta_0(\times10^{12})$ (mol cm^{-2})	$\theta_1(\times10^{9})$ (mol cm^{-2})	θ_2 ($\times10^{9}$) (mol cm^{-2})
−0.650	230	0.44	0.24	1.3	0.1	0.2
−0.600	300	0.54	0.33	1.7	0.1	1.6
−0.585	490	0.89	0.43	3.6	2.0	4.1
−0.585[a]	8700	3.80	6.02	1.6	3.8	2.4
−0.555	550	1.10	0.59	3.5	1.8	3.3
−0.535	710	1.23	0.62	3.5	2.0	3.9

[a]In the presence of chloride (KCl 0.1 M) (same experimental conditions as in Fig. 4)

According to the values in the literature of $b_1 = 13$ V^{-1} and $b_2 = 8$ V^{-1} [36], Eqs. (27), (28), (29) and (30) allow us to obtain the values of k_1, k_2, k_3 and θ_0 in a simple manner. These values are listed in Table 2. Also θ_1 and θ_2 values have been calculated assuming that the system reaches the steady state. The values obtained for θ_0 are relatively small if compared with θ_1 values, as is expected for a fast dissolution process. θ_2 values are relatively high, which is consistent with the important role of Ni(II) species in the nickel electrodissolution process.

The dependence of k_1 and k_2 on the potential has been plotted in Fig. 3 in order to check the consistency of the calculation procedure. From the slope of this plot b_i values are recalculated for each electron transfer. The values obtained for $b_1 = 15 \pm 2$ V^{-1} and $b_2 = 8 \pm 1$ V^{-1} are very close to values used in order to solve the simplified equation system.

Moreover, as seen in Table 2, the k_3 value is smaller than k_1 and k_2 in all the potential range studied. The dependence of k_3 on the potential could be explained if the transport of Ni^{2+} to the solution is a migration; however, this point requires further studies since neither the solubilization and transport of Ni^{2+} from the surface to the solution nor the other paths of the assumed mechanism (Eqs. 1, 2 and 3) are really elementary steps. At the tested conditions of Fig. 3, the capacitive loop at low frequencies is directly related to the value of k_3 by Eq. (29), since the time constant R_1C_1 is lower than R_2C_2.

In particular, it is widely known that anions play an important role in the kinetics of anodic dissolution of metals. In the case of the nickel dissolution, the kinetic parameters calculated by means the proposed procedure depend on the previous history of the electrode, the hydrodynamic conditions of the electrode as well as on the composition of the aqueous media. When chloride anions are present, the dissolution of nickel is favored and pitting of the surface appears [8, 38, 39]. An inductive loop is observed in the Nyquist plots at low frequencies instead of the capacitive loop, as can be seen in Fig. 4. In this way, the behavior at low frequencies is inductive in these experimental conditions as occurs in the anodic dissolution of zinc [37]. Therefore, and from

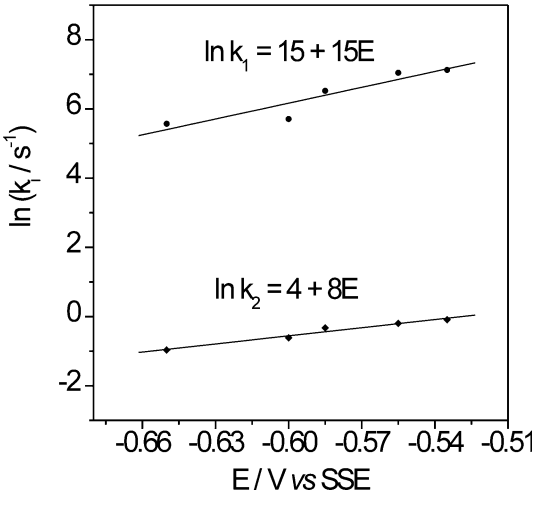

Fig. 3 Dependence of the calculated constant rates of the two electron transfers steps on the potential in the same experimental conditions as in Fig. 2

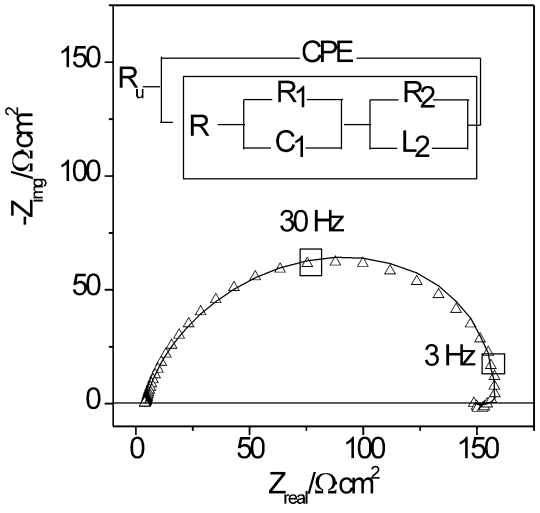

Fig. 4 Shape of Nyquist impedance plot in the presence of chloride within the acid solution. $E_0 = -585$ mV; 0.245 M K_2SO_4; 5×10^{-3} M H_2SO_4; 0.1 M KCl; pH = 2.7; $T = 298$ K. *Solid line* indicates the fitting to the equivalent circuit. $A = 126/\mu F\ cm^{-2}\ s^{\alpha-1}$; $\alpha = 0.80$; $R = 3\ \Omega\ cm^2$; $R_1 = 147\ \Omega\ cm^2$; $C_1 = 2\ \mu F\ cm^{-2}$; $R_2 = 29\ \Omega\ cm^2$; $L_2 = 3$ H cm^{-2}

similar assumptions to those used to deduce the system of equations (Eqs. 27, 28, 29 and 30), the electrical elements of the equivalent circuit can be related to the kinetic magnitudes of the anodic dissolution mechanism (see Appendix 2). These kinetic parameters are collected in Table 2. It is observed that the rate constants for all elemental steps have increased, but in this case $k_2 < k_3$ (see Table 2) and the surface concentration of Ni(I) increases with respect to the experimental case when chloride is absent in the medium. Therefore, and according to previous analysis of similar faradaic impedance functions, the capacitive or inductive nature of the low frequencies loop can be explained on the basis of the k_2/k_3 ratio which also implies the highest or lowest values for the surface concentration of intermediate species.

Conclusion

The analysis of mass/electrical charge ratio during the EQCM experiments proved that nickel electrodeposition takes place jointly with a pronounced hydrogen evolution. In addition, higher values of this ratio during the oxidation peak are explained by the presence of Ni(I) species on the nickel metal surface.

A procedure is proposed and analyzed to obtain kinetic parameters from the fitting of experimental data to the equivalent circuit. The dependence of kinetic constants on the applied potential is similar to that expected from b_1 and b_2 parameters obtained from other electrochemical techniques.

Finally, if chloride anions are present in the solution, an inductive loop appears at low frequencies instead of the capacitive loop. This result is explained from the values obtained for $k_2 < k_3$.

Therefore, this procedure is useful for characterizing the anodic dissolution of nickel by the use of equivalent circuits since a physical meaning can be attributed to all elements.

Acknowledgements This work has been supported by CICyT-Mat/2000-0-P4. D. Giménez-Romero acknowledges a Fellowship from the Generalitat Valenciana (FPI program). J. Gregori acknowledges a Fellowship from the Spanish Education Ministery (FPU program). J.J. García-Jareño acknowledges the financial support of the program "Ramón y Cajal" from the Spanish Science and Technology Ministry.

Appendix 1

A mathematical method, similar to that used by Diard et al. [40, 41] for the Volmer–Heyrovsky reduction mechanism, was used for obtaining the theoretical impedance function of the anodic dissolution of the metal. It can be considered that a metal dissolves by means of two consecutive electron transfers followed by a transport step, according to the reaction scheme:

$$\mathrm{Me}(0) \xrightarrow{r_1} \mathrm{Me(I)} + \mathrm{e}^- \tag{A1}$$

$$\mathrm{Me(I)} \xrightarrow{r_2} \mathrm{Me(II)} + \mathrm{e}^- \tag{A2}$$

$$\mathrm{Me(II)} \xrightarrow{r_3} \mathrm{Me}^{2+} \tag{A3}$$

where r_1, r_2 and r_3 are the reaction rates for each elementary step. Me(I) and Me(II) are the reaction intermediates.

The charge balance at the electrode surface defines the faradaic current:

$$\frac{i_F}{AF} = r_1 + r_2 \tag{A4}$$

where A and F are the electrode surface and the Faraday constant, respectively. The mass balance at the electrode surface, for each reaction intermediate, is described by the equations:

$$\frac{\mathrm{d}\theta_1}{\mathrm{d}t} = r_1 - r_2 \tag{A5}$$

$$\frac{\mathrm{d}\theta_2}{\mathrm{d}t} = r_2 - r_3 \tag{A6}$$

$$\theta_0 + \theta_1 + \theta_2 = \theta^0 \tag{A7}$$

where θ_0, θ_1 and θ_2 are the surface concentrations of Me(0), Me(I) and Me(II) species at the electrode surface and θ^0 is the initial concentration of free sites at the electrode surface. r_1, r_2, r_3, θ_0, θ_1 and θ_2 will be a function of potential E and θ_i. If each elementary step obeys kinetics of first order, it can be expressed as:

$$r_1 = k_1\theta_0 \tag{A8}$$

$$r_2 = k_2\theta_1 \tag{A9}$$

$$r_3 = k_3\theta_2 \tag{A10}$$

If a small sinusoidal perturbation of potential is applied around a defined steady state at a potential E_0, we can write the Taylor expansion for Eqs. (A4), (A5), (A6) and (A7) around this steady state in the Laplace plane. If the amplitude of the potential perturbation is small, only the terms of first order need be considered:

$$\frac{\Delta i_F}{AF} = \left(\frac{\partial r_1}{\partial E} + \frac{\partial r_2}{\partial E}\right)\Delta E - \frac{\partial r_1}{\partial \theta_0}\Delta\theta_2 + \left(\frac{\partial r_2}{\partial \theta_1} - \frac{\partial r_1}{\partial \theta_0}\right)\Delta\theta_1 \tag{A11}$$

$$\left(\frac{\partial r_1}{\partial \theta_0} + \frac{\partial r_2}{\partial \theta_1} + p\right)\Delta\theta_1 = \left(\frac{\partial r_1}{\partial E} - \frac{\partial r_2}{\partial E}\right)\Delta E - \frac{\partial r_1}{\partial \theta_0}\Delta\theta_2 \tag{A12}$$

$$\left(\frac{\partial r_3}{\partial \theta_2} + p\right)\Delta\theta_1 = \frac{\partial r_2}{\partial E}\Delta E + \frac{\partial r_2}{\partial \theta_1}\Delta\theta_1 \tag{A13}$$

where $p = j\omega$ is the Laplace variable. Dividing each term of Eqs. (A11), (A12) and (A13) by Δi_F an

equation system for $Z_F = \Delta E/\Delta i_F$, $\Delta\theta_1/\Delta i_F$ and $\Delta\theta_2/\Delta i_F$ is defined, where Z_F is the faradaic impedance which can be determined by means of the Kramer's rule:

$$FAZ_F = \frac{\begin{vmatrix} 1 & \frac{\partial r_2}{\partial\theta_1} - \frac{\partial r_1}{\partial\theta_0} & -\frac{\partial r_1}{\partial\theta_0} \\ 0 & -\left(\frac{\partial r_1}{\partial\theta_0} + \frac{\partial r_2}{\partial\theta_1} + p\right) & -\frac{\partial r_1}{\partial\theta_0} \\ 0 & \frac{\partial r_2}{\partial\theta_1} & -\left(\frac{\partial r_3}{\partial\theta_2} + p\right) \end{vmatrix}}{\begin{vmatrix} \frac{\partial r_1}{\partial E} + \frac{\partial r_2}{\partial E} & \frac{\partial r_2}{\partial\theta_1} - \frac{\partial r_1}{\partial\theta_0} & -\frac{\partial r_1}{\partial\theta_0} \\ \frac{\partial r_1}{\partial E} - \frac{\partial r_2}{\partial E} & -\left(\frac{\partial r_1}{\partial\theta_0} + \frac{\partial r_2}{\partial\theta_1} + p\right) & -\frac{\partial r_1}{\partial\theta_0} \\ \frac{\partial r_2}{\partial E} & \frac{\partial r_2}{\partial\theta_1} & -\left(\frac{\partial r_3}{\partial\theta_2} + p\right) \end{vmatrix}} \tag{A14}$$

Appendix 2

When chloride ion is present in the acid medium the experimental impedance spectra are fitted to the equivalent circuit of Fig. 4. The faradaic impedance function for this equivalent circuit is:

$$Z_F = \frac{R_2(R+R_1) + ((L_2(R+R_1+R_2) + RR_1R_2C_1)j\omega - (R_1C_1L_2(R+R_2))\omega^2}{R_2 + (R_1C_1R_2 + L_2)j\omega - (R_1C_1L_2)} \tag{A15}$$

If Eq. (A15) is compared with Eq. (11), the following equation system can be written:

$$\frac{\frac{\partial r_1}{\partial\theta_0}\frac{\partial r_2}{\partial\theta_1} + \left(\frac{\partial r_1}{\partial\theta_0} + \frac{\partial r_2}{\partial\theta_1}\right)\frac{\partial r_3}{\partial\theta_2}}{2\frac{\partial r_2}{\partial E}\frac{\partial r_1}{\partial\theta_0}\frac{\partial r_3}{\partial\theta_2} + 2\frac{\partial r_1}{\partial E}\frac{\partial r_2}{\partial\theta_1}\frac{\partial r_3}{\partial\theta_2}} = F(R+R_1) \tag{A16}$$

$$\frac{\frac{\partial r_1}{\partial\theta_0} + \frac{\partial r_2}{\partial\theta_1} + \frac{\partial r_3}{\partial\theta 2}}{2\frac{\partial r_2}{\partial E}\frac{\partial r_1}{\partial\theta_0}\frac{\partial r_3}{\partial\theta_2} + 2\frac{\partial r_1}{\partial E}\frac{\partial r_2}{\partial\theta_1}\frac{\partial r_3}{\partial\theta_2}} = F\frac{(L_2(R+R_1+R_2) + RR_1R_2C_1)}{R_2} \tag{A17}$$

$$\frac{\frac{\partial r_1}{\partial\theta_0}\frac{\partial r_2}{\partial E} + 2\frac{\partial r_1}{\partial E}\frac{\partial r_2}{\partial\theta_1} + \frac{\partial r_1}{\partial E}\frac{\partial r_3}{\partial\theta_2} + \frac{\partial r_2}{\partial E}\frac{\partial r_3}{\partial\theta_2}}{2\frac{\partial r_2}{\partial E}\frac{\partial r_1}{\partial\theta_0}\frac{\partial r_3}{\partial\theta_2} + 2\frac{\partial r_1}{\partial E}\frac{\partial r_2}{\partial\theta_1}\frac{\partial r_3}{\partial\theta_2}} = \frac{R_2R_1C_1 + L_2}{R_2} \tag{A18}$$

$$\frac{\frac{\partial r_1}{\partial E} + \frac{\partial r_2}{\partial E}}{2\frac{\partial r_2}{\partial E}\frac{\partial r_1}{\partial\theta_0}\frac{\partial r_3}{\partial\theta_2} + 2\frac{\partial r_1}{\partial E}\frac{\partial r_2}{\partial\theta_1}\frac{\partial r_3}{\partial\theta_2}} = \frac{R_1C_1L_2}{R_2} \tag{A19}$$

$$\frac{1}{2\frac{\partial r_2}{\partial E}\frac{\partial r_1}{\partial\theta_0}\frac{\partial r_3}{\partial\theta_2} + 2\frac{\partial r_1}{\partial E}\frac{\partial r_2}{\partial\theta_1}\frac{\partial r_3}{\partial\theta_2}} = F\frac{R_1L_2C_1(R+R_2)}{R_2} \tag{A20}$$

which can be simplified as in the previous case (two capacitive loops). If R and C_1 are very low and if it is considered that $k_1 \gg k_2, k_3$, the following equation system is obtained:

$$\frac{k_2 + k_3}{2k_1k_3b_2\theta_0} = FR_1 \tag{A21}$$

$$\frac{1}{2k_1k_3b_2\theta_0} = F\frac{(R_1+R_2)L_2}{R_2} \tag{A22}$$

$$\frac{1}{2k_3} = \frac{L_2}{R_2} \tag{A23}$$

$$\frac{b_1 + b_2}{2k_1k_3b_2} = \frac{R_1C_1L_2}{R_2} \tag{A24}$$

References

1. Arvía AJ, Posadas D (1975) In: Bard AJ (ed) Encyclopedia of electrochemistry of the elements, vol 3. Marcel Dekker, New York, p 211
2. Sato N, Okamoto G (1981) In: Bockris JO, Conway BE, Yeager E, White RE (eds), Electrochemical materials science, vol. 4. Plenum, New York, p 193
3. Real SG, Vilche JR, Arvía AJ (1980) Corros Sci 20:563
4. Barbosa MR, Real SG, Vilche JR, Arvía AJ (1988) J Electrochem Soc 135:1077
5. MacDougall B (1979) J Electrochem Soc 126:919
6. Abd El Rehim SS, Abd El Wahaab SM, Abd El Meguid EA (1986) Surf Coat Technol 29:325
7. Jouanneau A, Keddam M, Petit MC (1976) Electrochim Acta 21:287
8. Barbosa MR, Bastos JA, Gacía-Jareño JJ, Vicente F (1998) Electrochim Acta 44:957
9. Keddam M, Takenouti H, Yu N (1985) J Electrochem Soc 132:2561
10. Keddam M (1995) In: Marcus P, Oudar J (eds), Corrosion mechanism in theory and practice. Marcel Dekker, New York, pp 55–122
11. Itagaki M, Nakazawa H, Watanabe K, Noda K (1997) Corros Sci 39:901
12. Giménez-Romero D, García-Jareño JJ, Vicente F (2003) J Electroanal Chem 558:25
13. Giménez-Romero D, García-Jareño JJ, Vicente F (2002) Electrochem Commun 4:613
14. Shao HB, Wang JM, Zhang Z, Zhang JQ, Cao CN (2003) J Electroanal Chem 549:145
15. Bard AJ, Faulkner LR (2001) Electrochemical methods. fundamentals and applications, 2nd edn. Wiley, New York, pp 316–370
16. Macdonald DD (1990) Electrochim Acta 35:1509
17. Macdonald DD (1977) Transient techniques in electrochemistry. Plenum, New York, pp 229–311
18. Epelboin I, Gabrielli C, Keddam M (1975) Corros Sci 15:155
19. Vanmaekelbergh D, Erné BH (1999) J Electrochem Soc 146:2488
20. Berthier F, Diard JP, Michel R (2001) J Electroanal Chem 510:1
21. Gabrielli C (1983) Identification of electrochemical processes by frequency response analysis. Solartron Instrumentation Group, Farnborough
22. Keddam M, Mattos OR, Takenouti H (1981) J Electrochem Soc 128:257
23. Keddam M, Mattos OR, Takenouti H (1981) J Electrochem Soc 128:266
24. Sanchez S, Picard GS (1996) Electrochim Acta 41:2035
25. Péter L, Arai J, Akahoshi H (2000) J Electroanal Chem 582:125
26. Armstrong RD, Firman RE, Thirsk HR (1973) Faraday Discuss 56:44
27. Macdonald JR (1992) Solid State Ionics 58:97
28. Vicente F, García-Jareño JJ, Sanmatías A (2000) Procesos Electródicos del NAFIÓN y del Azul de Prusia sobre electrodo

transparente de óxido de indio-estaño: un modelo de electrodo multicapa. Moliner-40, Burjassot
29. Lachenwitzer A, Magnussen OM (2000) J Phys Chem B 104:7424
30. Giménez D, García-Jareño JJ, Vicente F Materiales y Procesos Electródicos I (2002). INSDE, València, pp 65–84
31. Sauerbrey G (1959) Z. Physik 155:206
32. Song KD, Kim KB, Han SH, Lee HK (2003) Electrochem Commun 5:460
33. Lachenwitzer A, Morin S, Magnussen OM, Behm RJ (2001) Phys Chem Chem Phys 3:3351
34. Wiart R (1990) Electrochim Acta 35:1587
35. Gabrielli C, Keddam M (1996) Electrochim Acta 41:957
36. Jouanneau A, Petit MC (1976) J Chim Phys 73:82
37. Giménez-Romero D, García-Jareño JJ, Vicente F (2003) J Electroanal Chem (in press)
38. Real SG, Barbosa MR, Vilche JR, Arvía AJ (1990) J Electrochem Soc 137:1696
39. Gregori J, Agrisuelas J, Gimenez D, Peña MP, Garcia-Jareno JJ, Vicente F (2003) Rev Metal 39:346
40. Diard J-P, Le Gorrec B, Montella C (1996) Cinétique Électrochimique. Collection Méthodes, Hermann, Paris
41. Diard J-P, Le Gorrec B, Montella C, Montero-Ocampo C (1993) J Electroanal Chem 352:1